A generalized model of TiO_x-based memristive devices and its application for image processing*

Jiangwei Zhang(张江伟)[1,2,3], Zhensen Tang(汤振森)[1,2], Nuo Xu(许诺)[1,2,4], Yao Wang(王耀)[2], Honghui Sun(孙红辉)[1,2], Zhiyuan Wang(王之元)[1,2], and Liang Fang(方粮)[1,2,†]

[1] *State Key Laboratory of High Performance Computing, National University of Defense Technology, Changsha* 410073, *China*
[2] *School of Computer, National University of Defense Technology, Changsha* 410073, *China*
[3] *Department of Electrical and Computer Engineering, University of Pittsburgh, Pittsburgh, PA* 15261, *USA*
[4] *Department of Material Science and Engineering, College of Engineering, Seoul National University, Seoul* 151-744, *Republic of Korea*

(Received 8 March 2017; revised manuscript received 18 May 2017; published online 27 July 2017)

Memristive technology has been widely explored, due to its distinctive properties, such as nonvolatility, high density, versatility, and CMOS compatibility. For memristive devices, a general compact model is highly favorable for the realization of its circuits and applications. In this paper, we propose a novel memristive model of TiO_x-based devices, which considers the negative differential resistance (NDR) behavior. This model is physics-oriented and passes Linn's criteria. It not only exhibits sufficient accuracy (IV characteristics within 1.5% RMS), lower latency (below half the VTEAM model), and preferable generality compared to previous models, but also yields more precise predictions of long-term potentiation/depression (LTP/LTD). Finally, novel methods based on memristive models are proposed for gray sketching and edge detection applications. These methods avoid complex nonlinear functions required by their original counterparts. When the proposed model is utilized in these methods, they achieve increased contrast ratio and accuracy (for gray sketching and edge detection, respectively) compared to the Simmons model. Our results suggest a memristor-based network is a promising candidate to tackle the existing inefficiencies in traditional image processing methods.

Keywords: memristor modeling, memristor-based network, gray sketching, edge detection

PACS: 05.45.–a, 87.85.dq, 95.75.Mn, 05.45.Tp **DOI:** 10.1088/1674-1056/26/9/090502

1. Introduction

With the coming era of the big-data, the size of produced and stored data in 2020 is expected to approach 44000 exabytes ($\approx 10^{18}$ bytes),[1] among which image data will account for a major portion.[2] Since image processing is both computationally and data demanding, the challenge to enhance its efficiency becomes a paramount concern of this field.[3]

The memristor, which was first fabricated in Hewlett Packard (HP) Labs in 2008,[4] has the potential to break the efficiency bottleneck of image processing applications. It is a two-terminal passive device that has several distinctive properties, such as scalability, nonvolatility, and high density, which make it a promising candidate for future memory.[5,6] Its capability not only to function in the analog space with neural networks, but also to act as a form of binary storage in traditional computation means it has significant potential to tackle many future computing problems.[7–9]

The availability of highly accurate, general and predictive memristive models is crucial for investigation of nonlinear dynamics of memristor-based circuits.[10,11] Memristive models, usually represented by differential equations that are directly available for circuit simulations, define specific methods to compute the responses to a given stimulus. To date, several models have been reported.[12–18] It is necessary to compare, evaluate, and classify them in advance in order to quickly select an appropriate model for a specific application. Recently, Linn *et al.*[19] reported three experiment-based criteria that can be used to evaluate the quality of two classes of models. The first class of models are linear ion drift models, which build upon Strukov's initial memristive model[4,20] with different window functions, but have limited predictability due to the nonlinear traits of the switching kinetics.[19] The second class are physics-oriented models, represented by the Simmons,[13] Chang's,[15] and Yang's[17,21] models, which successfully pass Linn's criteria. From the perspective of a circuit designer, a model should be efficient enough to reflect various properties of devices with a few simple functions. However, existing models are a trade-off between complexity and accuracy. The Simmons model is accurate, but too complex for circuit design. Chang's and Yang's models are computationally efficient, but not accurate enough. Another deficiency of these models is their neglect of some physical phenomena, such as negative differential resistance (NDR),[22] long-term potentiation (LTP), and long-term depression (LTD) behaviors.

In this paper, an experiment-based memristive model that is accurate and computationally efficient for circuit design is

*Project supported by the National Natural Science Foundation of China (Grant Nos. 61332003 and 61303068) and the Natural Science Foundation of Hunan Province, China (Grant No. 2015JJ3024).

†Corresponding author. E-mail: lfang@nudt.edu.cn

© 2017 Chinese Physical Society and IOP Publishing Ltd

proposed, which passes Linn's criteria and can also describe the NDR and LTP/LTD behaviors. As compared to the memristive models previously reported, it achieves lower latency (below half the VTEAM[16] model) and preferable generality without sacrificing accuracy. On the basis of memristive models, we propose novel methods for gray sketching and edge detection operations, which can greatly enhance the efficiency by avoiding the time-consuming calculations of complex nonlinear functions. The proposed model is verified to surpass the Simmons model for the aforementioned image processing applications, and our results suggest that a memristor based network may provide a new solution to tackle the efficiency problem of image processing.

The rest of the paper is organized as follows. Section 2 gives a brief introduction of fabrication procedure and characterizations of TiO_x-based memristive device. In Section 3, a general memristive model is proposed and evaluated with strict evaluation criteria, and a comparison of accuracy and complexity is provided between the proposed model and previously published memristive models. Moreover, the proposed model is fitted to experimental data of memristive devices and the previous memristive models to show its generality. In Section 4, the predictability of the LTP/LTD behavior is compared among the memristive models, and applications of gray sketching and edge detection are implemented based on these models. Finally, we summarize this work in Section 5.

2. TiO_x-based memristive devices

TiO_x-based memristors are prototypical for valence change mechanism (VCM) devices[23] whose resistive switching behavior is attributed to the formation and dissolution of oxygen-deficient filaments in transition metal oxides.[24] To examine this behavior first hand, an Au/Ti/TiO_2/Au memristor-based crossbar array (16×16) was fabricated.[25] Figure 1 shows the I–V characteristics of our devices with 50 hysteresis loops. These 50 hysteresis loops are nearly overlapped, demonstrating the repeatability of the device. For each loop, the NDR behavior appears during the RESET process. The upper inset is a schematic diagram of the devices, from bottom to top, including an Au bottom electrode (BE), a TiO_2 thin film layer, a Ti thin film layer, and an Au top electrode (TE). The lower inset is the input voltage applied to the TE, with the selected BE grounded and the other unselected electrodes floated. To avoid sneak-path current leakage, any memristive devices investigated simultaneously in the 16×16 array should not constitute a rectangle.[25,26] The input signal was a triangular voltage sweep of amplitude -2 V/2 V. During the SET process, a 1-mA current compliance was added, whereas there was no current restriction during the RESET process.

Detailed device fabrication methods and experimental tests were presented in our previous work.[25,27]

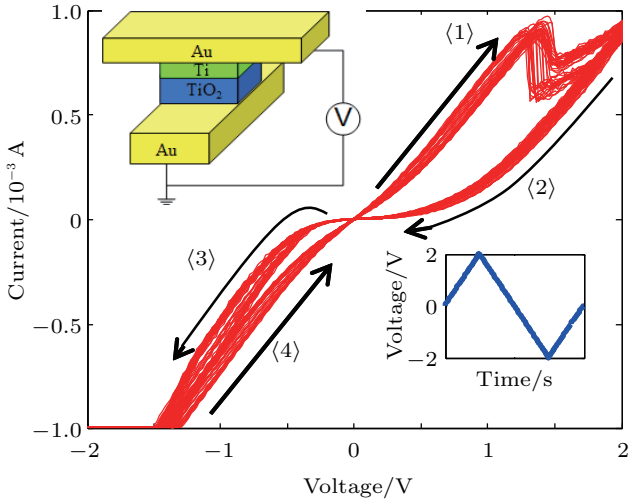


Fig. 1. (color online) Reversible and nonvolatile switching of Au/Ti/TiO_2/Au devices. The upper inset shows a schematic diagram of the crossbar devices with an Au bottom electrode (BE, 25 nm), a TiO_2 thin film (40 nm), an adhesion Ti layer (5 nm) and an Au top electrode (TE, 35 nm). The red curves represent 50 experimental switching loops, which show a high level of repeatability. For each interval, the device stays in low resistance state (LRS) at $\langle 1 \rangle$ initially and switches to high resistance state(HRS) at $\langle 2 \rangle$. Then, it switches back to LRS at $\langle 3 \rangle$ and then finally returns to the initial LRS at $\langle 4 \rangle$. It is obvious that before the end of $\langle 1 \rangle$, the curve shows the negative differential resistance (NDR) behavior.

3. Memristive models

Generally, a voltage-controlled memristive system[28,29] is represented by

$$\dot{X} = f(X,V), \tag{1}$$

$$I = G(X,V), \tag{2}$$

where X is an internal state variable, V is the voltage, I is the current, and $G(X,V)$ is the memconductance. From Eq. (2), it can be observed that the memconductance varies depending on the state variable and the current voltage.

An available memristive model should abstract, parametrize, and predict the behaviors of devices under a given stimulus. In this section, we propose a novel memristive model and compare it with previously reported models in respects of accuracy, complexity, and predictability.

3.1. Proposed model

In the practical case, the charged mobile ions (e.g., oxygen ions in TiO_2) would drift under the influence of the electric field, leading to variations of the inner state variable. The relationship between electric field intensity and moving speed of ions is not linear, but always exponential. In addition, due to the high mobility of oxygen vacancies, diffusion effects of the charged mobile ions should be considered as well.

On the basis of various experimental tests and analysis, Chang's model[15] defines the inner state variable by integrating the drifting and diffusing effects in a single equation. We define the inner state variable in a similar way as

$$\dot{X} = \begin{cases} \alpha_1 \sinh \beta_1 V - \gamma X, & V > 0, \\ \alpha_2 \sinh \beta_2 V - \gamma X, & V < 0, \end{cases} \tag{3}$$

where α_1, α_2, β_1, and β_2 are all positive parameters related to the drift effect and γ is a positive parameter related to the diffusion effect.

However, a memristive device may not only exhibit these effects; in this case, the contributions of the NDR behavior should not be ingored. At low resistance states, conductive filaments (CF) have formed in transition metal oxides of memristive devices. When joule heating of the devices is excessively high, it may lead to gradual ruptures of the filaments.[22,30] This morphological variation of the filaments would then raise the resistances of the devices, removing the NDR behavior as the device generates less heat and the joule heating dissipates. Therefore, the NDR behavior is related to the history of electric field applied to the devices and may only exist at some interval of integrated external electric field. In order to model this behavior, we introduce a thermal variable E

$$E = \int VI \mathrm{d}t, \tag{4}$$

and define its valid interval $[E_{\min}, E_{\max}]$. The RESET process is always described as an exponential relationship between the inner state variable and the electric field.[31–33] The NDR behavior appears during the RESET process, so the NDR window can be defined as an exponential formula

$$W_{\mathrm{NDR}} = \begin{cases} \mathrm{e}^{-(E-E_{\mathrm{c}})/\sigma}, & E_{\min} < E < E_{\max}, \\ 1, & \text{others}, \end{cases} \tag{5}$$

where E_{c} is a bias parameter and σ is a regulating parameter. Note that if the NDR behavior does not appear, as is the most common case, one can adopt Eq. (3) to define the inner state variable.

For TiO_x-based devices, a Schottky barrier is always formed between titanium oxide film and the bottom layer, while an electron tunneling layer always develops when a positive voltage is applied to the top layer. To integrate these two effects, we define I–V equation as follows:

$$I = \begin{cases} X^{n_1} k_{\mathrm{on}_1} \sinh \dfrac{V}{v_{\mathrm{on}_1}} + (1 - X^{n_1}) k_{\mathrm{r}} \left(\mathrm{e}^{V/v_{\mathrm{r}}} - 1 \right), \\ \qquad V \geq 0, \\ X^{n_2} k_{\mathrm{on}_2} \sinh \dfrac{V}{v_{\mathrm{on}_2}} + (1 - X^{n_2}) k_{\mathrm{off}} \sinh \dfrac{V}{v_{\mathrm{off}}}, \\ \qquad V < 0, \end{cases} \tag{6}$$

where k_{on_1}, v_{on_1}, k_{on_2}, and v_{on_2} are fitting parameters characterizing ON state at different input voltage polarities, k_{r}, v_{r}, k_{off}, and v_{off} are positive parameters accounting for OFF state, and n_1, n_2 are positive parameters to regulate X. In Eq. (6), both expressions include the tunneling term (the first term) and the Schottky term (the second term). According to Eqs. (1) and (2), the proposed model is the combination of the I–V equation (6), the internal state variable equation (3), and the NDR window (Eq. (5)).

The proposed model is distinctive. The Simmons model uses a tunneling junction with a series resistor to model a memristive device. The inner state variable (X) of the model describes the width of the tunneling junction. In contrast, X of the proposed model represents an area index, i.e., the number of CFs or the area of the conductive region. Hence, these two models have different X descriptions. The proposed model is also different from Chang's model. They have different formula expressions of X and different I–V functions. The proposed model considers the NDR behavior, and uses two functions to describe the asymmetric electrical properties under both polar input voltage signals.

3.2. Evaluating the proposed model with Linn's criteria

A distinct characteristic of a memristive device is that its resistance can be controllably changed by a given electrical stimulus. The device can achieve a low resistance state (LRS) under a positive stimulus, while a high resistance state (HRS) can be obtained under a negative stimulus. The transition from LRS to HRS is called a "RESET" process, and the transition from HRS to LRS is called a "SET" process.

A memristive model is a dynamical system that can be used to predict device behaviors under any given input stimulus. The proposed model does not have any current or voltage threshold, because models with built-in fixed thresholds (currents or voltages) are not general enough and always lack predictability.[19] Though there are thermal thresholds accounting for the NDR behavior, they are dispensable when a memristive device does not exhibit this behavior. In the following analysis, we evaluate the proposed model with three strict criteria using Matlab. The parameters of the proposed model in this simulation are in the second colomn of Table 2 except that γ equals 25.

The first evaluation criterion is that, for a reasonable model, it should have the ability to predict the distinct I–V characteristics of a memristive device. Typically, there are four characteristics: an abrupt current increase during the SET process, a gradual RESET process of the VCM-based memristive devices, an I–V-plot that is asymmetric about the origin, and an observed increase in both SET and RESET voltages with a higher sweep rate. In Fig. 2(a), we see an abrupt current increases and a gradual current decrease during the SET and RESET processes, respectively. Meanwhile, the I–V curves of the proposed model are obviously asymmetric about the origin. Furthermore, figure 2(a) also exhibits I–V curves of the proposed model at triangular voltage sweeps with different sweep rates. As the sweep rates increase, the model presents higher SET and RESET voltages, consistent with the physical device. Therefore, the proposed model obeys the first evaluation criterion.

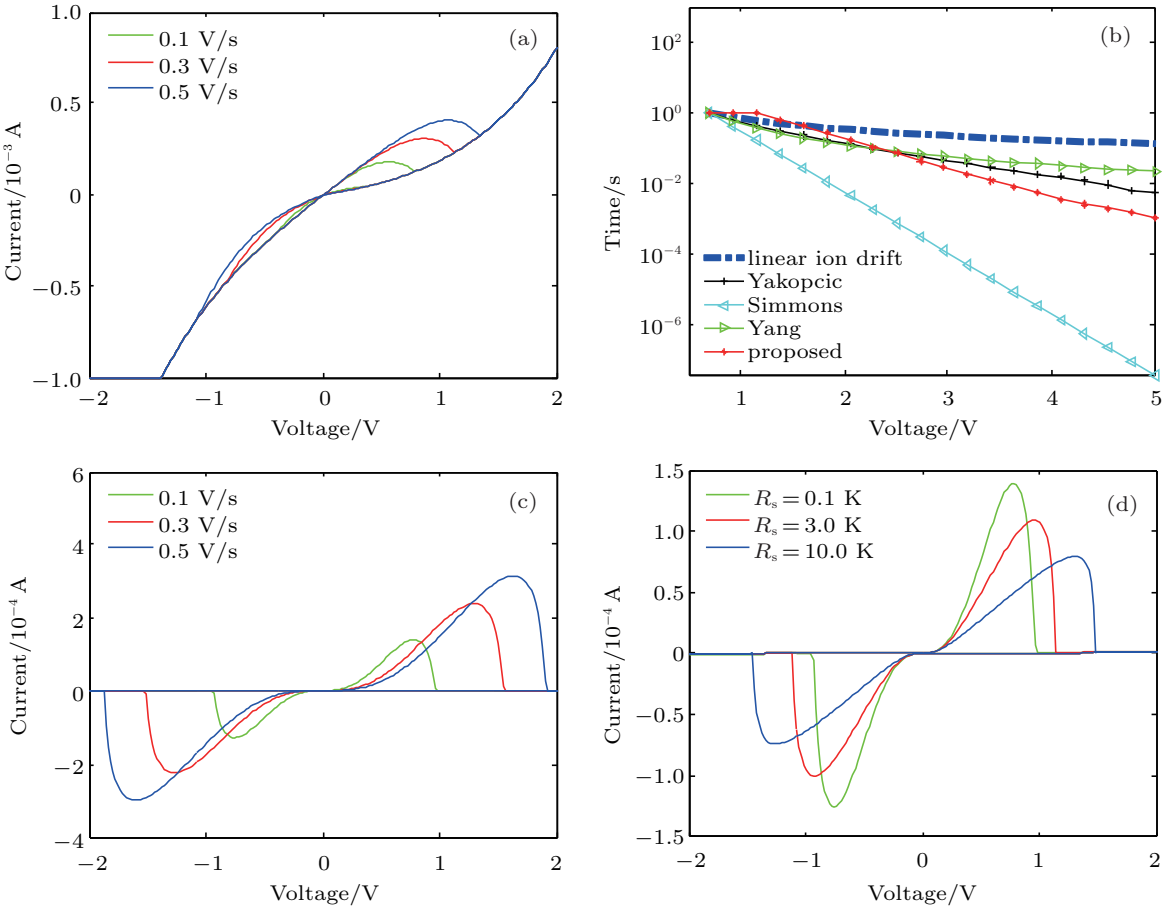


Fig. 2. (color online) Evaluation of the proposed model. (a) *I–V* curves at different sweep rates of sweep voltages. (b) SET time versus applied voltage amplitude. (c) *I–V* curves of anti-serial connection of two devices at different sweep rate of sweep voltages. (d) *I–V* curves of anti-serial connection of two devices with different serial resistances.

The second evaluation criterion is that, during fixed-voltage pulse tests, the relationship between SET time $t_{\rm set}$ and pulse amplitude $V_{\rm p}$ should be nonlinear due to the high nonlinearity of the switching kinetics. When checking this criterion, the first step is to initialize the device in the HRS state. Following this, positive voltage pulses are applied, and the transition time from the HRS state to the LRS state is recorded. In Fig. 2(b), we can see a basic trend. For each of the models, as the pulse amplitude increases, the SET time decreases, though the degree of nonlinearity varies. The initial SET time of the models, at a pulse amplitude of 0.7 V, is normalized for the sake of comparison. It is proved in Ref. [19] that, for each linear ion drift model, the SET time is inversely proportional to the pulse amplitude irrespective of any window function. The other four nonlinear models demonstrate that the SET time decreases by several orders of magnitude after increasing the pulse amplitude by only a factor of four. Among the four models, the Simmons model holds the highest degree of nonlinearity, followed by the proposed model, Yakopcic's model, and then Yang's model in sequence. Hence, the proposed model passes the second evaluation criterion with relatively high nonlinearity of the switching kinetics.

The third evaluation criterion can be validated by simulating the CRS behavior through two devices connected anti-serially. Theoretically, any change of the state variable of one device can be offset by the other one so that the resistance of the combined cell is constant. In Fig. 2(c), we show the *I–V* curves of an anti-serial connection of two devices at different voltage sweep rates. We see an overall low resistive state, namely ON state, at each sweep rate. Moreover, demonstrating the same characteristic which is shown in Fig. 2(a), the anti-serial connection of two devices presents higher SET and RESET voltages as the sweep rates increase. In Fig. 2(d), another important behavior is that the ON state is enlarged with a bigger series resistance, which is in line with previous reports.[34,35] Meanwhile, as the overall resistance becomes larger, the current flowing through the devices gets lower, which accords with Ohm's law. Consequently, our model passes the third evaluation criterion completely.

3.3. Comparison with memristive models

Ideally, a memristive model should reflect experimental data while being as fast and simple as possible. To compare the accuracy and complexity between the proposed model and the reference models, we fit these models to measured data by adjusting their parameters to minimize error functions.

To perform the fitting, we use Gradient Descent[36] and simulated annealing algorithms[37] to minimize the relative error function value. To reduce the possibility of local convergence of a single error function, we use two different error functions: the first error function is relative root mean squared error (RMS) as

$$e_{\mathrm{rms}} = \sqrt{\frac{1}{N}\left(\frac{\sum_{n=1}^{N}\left(V_{\mathrm{pro},n}-V_{\mathrm{ref},n}\right)^2}{\bar{V}_{\mathrm{ref}}^2}+\frac{\sum_{n=1}^{N}\left(I_{\mathrm{pro},n}-I_{\mathrm{ref},n}\right)^2}{\bar{I}_{\mathrm{ref}}^2}\right)}, \quad (7)$$

where N is the total number of samples, $V_{\mathrm{pro},n}$ and $I_{\mathrm{pro},n}$ are the characteristics of the nth sample of the model under examination, $V_{\mathrm{ref},n}$ and $I_{\mathrm{ref},n}$ are the characteristics of the nth sample of reference data, and $\bar{V}_{\mathrm{ref}}$ and $\bar{I}_{\mathrm{ref}}$ are the Euclidean norms of their respective reference data. The second error function, threshold adaptive exponential error (TAE), is

$$e_{\mathrm{tae}} = k\frac{M}{N}\sum_{j=n_1}^{n_M}\exp\left(\frac{\left|I_{\mathrm{pro},j}-I_{\mathrm{ref},j}\right|-T}{\sigma}\right), \quad (8)$$

where k is a scale parameter, T is a threshold value, σ is an adjustment parameter, M is the number of samples (among which n_1 and n_M are the first and last samples, respectively) whose absolute current errors between examined model and the reference data exceed T. Here, T is defined as

$$T = \mu(\max I_{\mathrm{ref}} - \min I_{\mathrm{ref}}), \quad (9)$$

where μ is a scale parameter.

During each fitting procedure, two related parameters are iterated and adjusted to minimize the error functions in Eqs. (7) and (8). To further avoid local convergence, parameters should be adjusted manually to make the error function values as small as possible. In practice, it is better to understand the meaning of each parameter in the processing model first and adopt proper initial values to simplify the fitting procedures and reduce the possibility of local convergence. We have adopted two tips to choose proper initial values: the first one is to discover relationships between the parameters by capturing typical states, for example, k_{on_1} and v_{on_1} of the proposed model have a relationship, in the LRS state at the beginning of $\langle 1\rangle$ in Fig. 1. In this case, if X equals 0, then $I'|_{V=0^+,X=0} = k_{\mathrm{on}_1}/v_{\mathrm{on}_1}$, which can be obtained from the measured data. Analogously, if X equals 1 at the end of $\langle 2\rangle$, then $I'|_{V=0^+,X=1} = k_{\mathrm{r}}/v_{\mathrm{r}}$. Further, if X equals 1 at the beginning of $\langle 3\rangle$, then $I'|_{V=0^-,X=1} = k_{\mathrm{off}}/v_{\mathrm{off}}$, and if X equals 0 at the end of $\langle 4\rangle$, then $I'|_{V=0^-,X=0} = k_{\mathrm{on}_1}/v_{\mathrm{on}_2}$. The second tip is to observe the voltage thresholds that can be used to define the thermal variable by integration.

In Fig. 3, fitting results to measured data for six different models are shown. The upper insets show the log-scale switching I–V curves. Among these models, in Figs. 3(a)–3(d), the Simmons, the VTEAM, Yang's and Chang's models are previously reported memristive models, which have different inner state variables, while the proposed models without and with NDR window are in Figs. 3(e) and 3(f), respectively. The Simmons model is an accurate current-controlled model, but we have changed it to the voltage-controlled mode and adjusted its parameters properly based on the measured data. The VTEAM model[16] is a simplified voltage-controlled mode of the Simmons model with several reasonable approximations to reduce complexity. Chang's and Yang's models[17] are compact nonlinear models whose I–V characteristics are a combination of hyperbolic sine and exponential functions. Only the VTEAM model[16] exhibits a built-in threshold voltage, which is a shortcoming in some practical uses, e.g., when predicting the LTP/LTD behavior. Comparisons of accuracy and complexity between the six models are presented in Table 1. According to both error functions, the proposed model with or without the NDR window exhibits sufficient accuracy, with the RMS error value lower than 1.5% and the TAE error value lower than 0.5%. Though the proposed model with the NDR window is more accurate than the one without the NDR window, it takes 13.4 times longer to run. According to the TAE error function, the Simmons model is the third most accurate model, following the two versions of the proposed model, though it has the second highest computation time. The deviations in the models from the measured data can be observed in Fig. 3; the proposed models most closely follow the measured data outside of the regions where NDR is active. The other models have not shown sufficient accuracies, irrespective of run time. Therefore, the proposed model without NDR window demonstrates remarkable accuracy given its complexity.

3.4. Fitting the proposed model to memristive devices and models

To test the generality and predictability of the proposed model, we fit the model to the reference models while keeping the original parameters of the reference models constant. The proposed model is further fit to measured data of two frequently-used devices to verify its predictability: an HfO_x-based device[38] and a TaO_x-based device.[39]

The fits of the proposed model to the aforementioned reference models and devices are shown in Fig. 4, and the corresponding parameters are listed in Table 2. The inset figures are the log-scale I–V curves for intuitive comparison in the logarithmic coordinate plane. All the parameters of the proposed model were allowed to vary for each fitting. The minimal values of the error functions are small, with the RMS error values lower than 1.5% and the TAE error values lower than 0.2%.

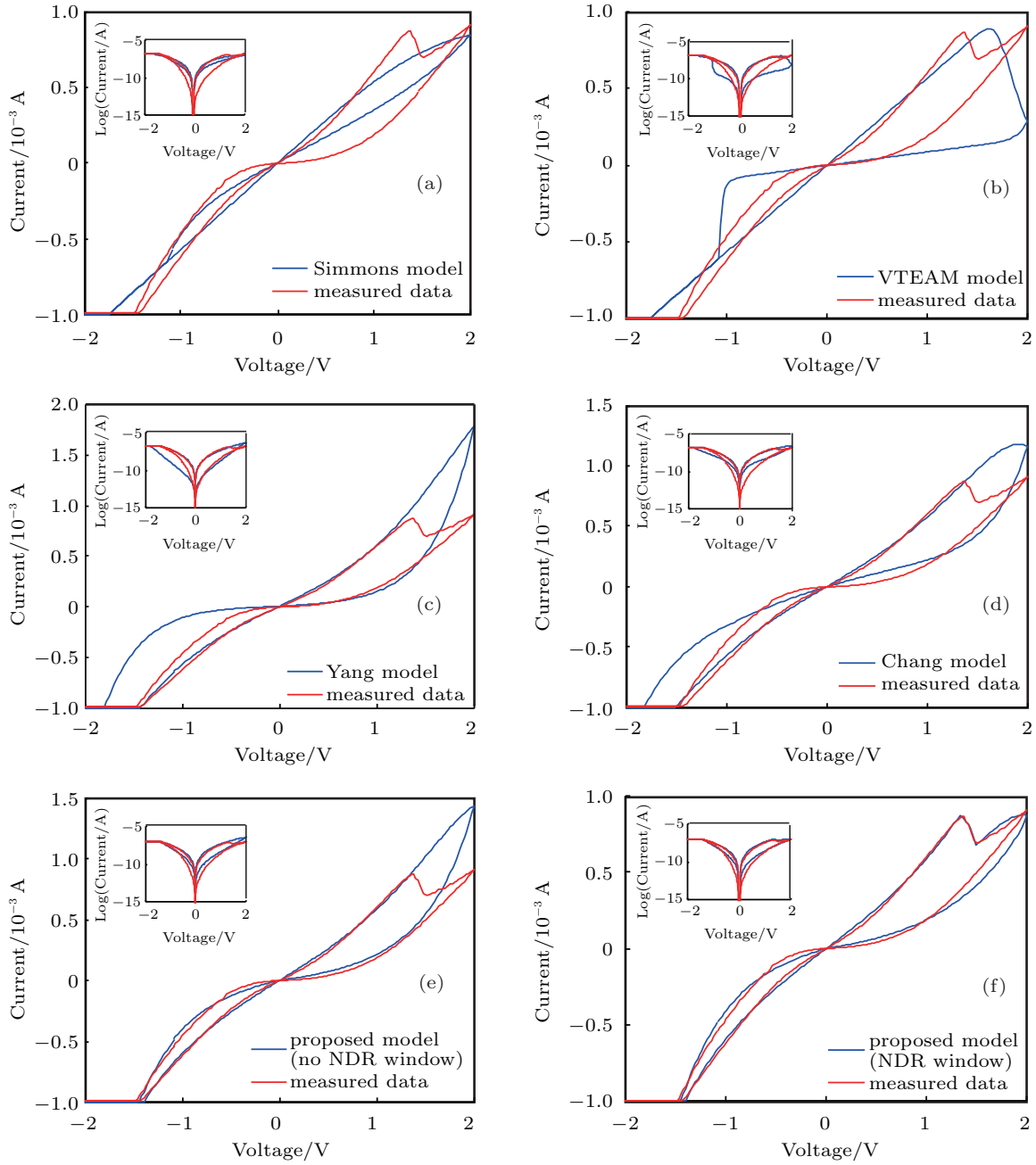


Fig. 3. (color online) Comparison between the memristive models. The upper insets show the log-scale switching *I*–*V* curves. (a) The Simmons model, (b) VTEAM model, (c) Yang's model, (d) Chang's model, (e) the proposed model without NDR window, and (f) the proposed model with NDR window.

Table 1. Comparison of different memristive models.

Models	σ_{RMS}/%	σ_{tae}/%	Run time/ms
The Simmons model	0.68	0.74	1.36
VTEAM model	1.52	0.89	0.27
Yang model	3.05	2.72	0.07
Chang model	2.16	2.38	0.09
Proposed model (No NDR window)	0.85	0.08	0.11
Proposed model(NDR window)	0.29	0.04	1.58

4. Simulations and applications

4.1. Simulation of LTP/LTD behavior

The conductance variation of memristive devices is analogous to the behavior of synapses in neuromorphic systems. In other words, the memristive conductance is gradually enlarged or reduced by applying consecutive positive or negative pulses, giving rise to long-term potentiation/depression (LTP/LTD). If a memristive model is valid, it should have the ability to predict the LTP and LTD behaviors of the devices. In this subsection, we focus on the simulation of the LTP/LTD behavior under consecutive fixed-voltage pulses with different pulse widths to compare the validity of the memristive models using Matlab.

In Fig. 5, we compare LTP/LTD responses produced by the Matlab simulation with the measured data of the HfO_x-based device in Ref. [38] under identical rectangular spikes. Though the measured data exhibit more fluctuations than its

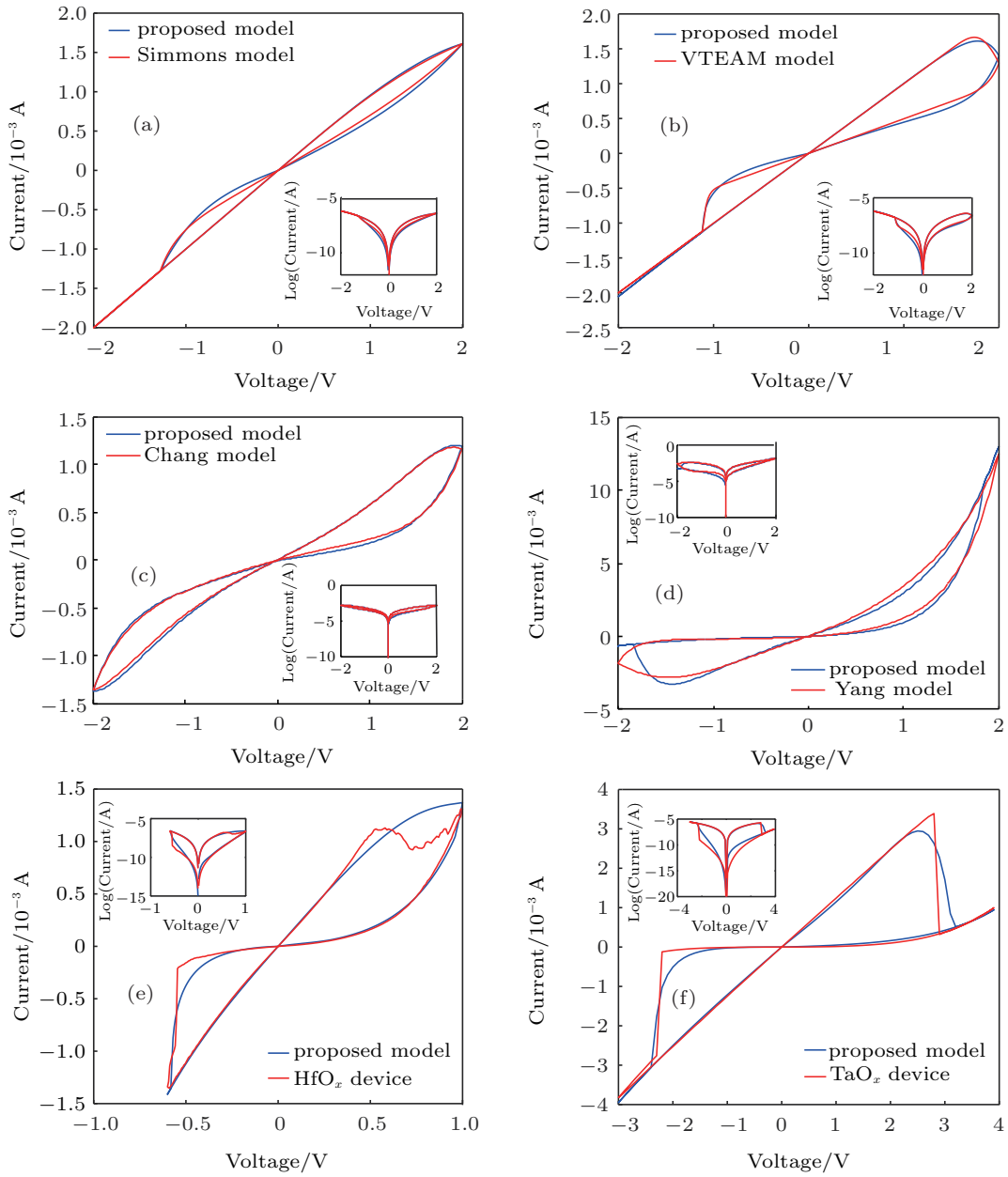


Fig. 4. (color online) Fit the proposed model to measured data and previously reported memristive models. The insets show the log-scale switching *I*–*V* curves. (a) The Simmons model, (b) VTEAM model, (c) Chang's model, (d) Yang's model, (e) HfOx-based device, and (f) TaOx-based device.

Table 2. Optimized parameters of the proposed model to memristive devices and other memristive models.

Devices & models	TiO_x device	HfO_x device	TaO_x device	The Simmons model	VTEAM model	Chang's model	Yang's model
k_{on_1}	4.5×10^{-4}	1.2×10^{-3}	2.2×10^{-3}	4×10^{-2}	5×10^{-3}	4.5×10^{-4}	2×10^{-4}
k_{on_2}	4.5×10^{-4}	1.2×10^{-3}	4.8×10^{-3}	4×10^{-2}	5×10^{-3}	4.5×10^{-4}	2×10^{-4}
k_{off}	10^{-4}	5×10^{-6}	1×10^{-5}	4×10^{-4}	3.5×10^{-5}	3×10^{-3}	1.5×10^{-4}
k_r	8.5×10^{-5}	3.5×10^{-5}	3.8×10^{-5}	1.2×10^{-4}	10^{-5}	3.5×10^{-4}	6×10^{-4}
v_{on_1}/V	0.9	0.6	2	40	5	0.9	0.8
v_{on_2}/V	0.9	0.6	4	40	5	0.9	0.8
v_{off}/V	0.5	5	5	0.4	0.4	10	0.4
v_r/V	0.85	0.28	1.2	1.5	1	2.5	3
α_1	59.75	375	214.2	100	0.25	60	5
β_1	1.731	2	1.3	0.9	4.7	1.73	4
α_2	59.75	75	214.2	100	2.5	60	5
β_1	1.731	6	1.9	2.5	7	1.73	4
γ	125	250	71.4	25	125	2.5	2.5
n_1	1	1	2	1	1	1	1
n_2	1	0.3	0.3	0.5	0.3	1	1
σ_{rms}/%	0.29	0.78	1.39	0.16	0.18	0.18	0.87
σ_{tae}/%	0.04	0.12	0.04	0	0.01	0.01	0.15

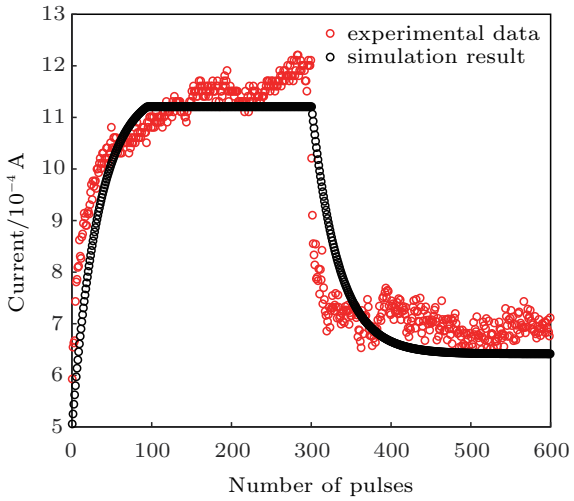


Fig. 5. (color online) A comparison of LTP/LTD responses between simulation results and experimental data of HfO_x device under trains of identical rectangular spikes described in Ref. [38]. Potentiation: voltage amplitude 0.55 V, time width 25 μs, rise and fall times 100 ns. Depression: voltage amplitude −0.7 V, time width 20 μs, rise and fall times 100 ns.

counterpart, the simulation results provide an accurate prediction with a very low error value of 0.31% in terms of relative RMS error.

The experimental data of the HfO_x-based[38] and other memristive devices previously reported[15,40–42] have shown that the change rate of the conductance tends to be smaller as the device approaches the HRS and LRS states in depression and potentiation operations, respectively. In Fig. 6, we also show the results of the LTP/LTD behavior based on the memristive models. The voltage pulse amplitude is 1.3 V and the pulse widths are 10 μs, 20 μs, and 30 μs. The parameters of the memristive models are the same as the ones in Fig. 3.

The models exhibit three common characteristics. First, the conductance of the models is not linearly related with the number of voltage pulses. Second, for both depression and potentiation operations, as the pulse width gets larger, fewer numbers of pulses are needed to switch the states. Finally, for the depression operation, as the models approach their LRS states, the change rate of the conductance gets smaller. These characteristics are consistent with the device behaviors in experimental tests.[15,40–42] On the other hand, the models have their distinct traits: to begin with, for the proposed and the Simmons models, the numbers of pulses needed in the potentiation operations are relatively fewer than the ones in the depression operations, which accords with the fact that the potentiation operation is always abrupt, whereas the depression operation is gradual for a VCM-based RRAM cell. However, Chang's and Yang's models do not obviously reflect this fact. Next, for the proposed and Chang's models, when approaching their LRS states in the potentiation operation, the change rate of the conductance gets smaller, while the Simmons model and Yang's model do not follow this principle. Finally, the proposed, Simmons, and Yang's models exhibit an obvious nonlinearity in the depression operation, while Chang's model is almost linear at each pulse width.

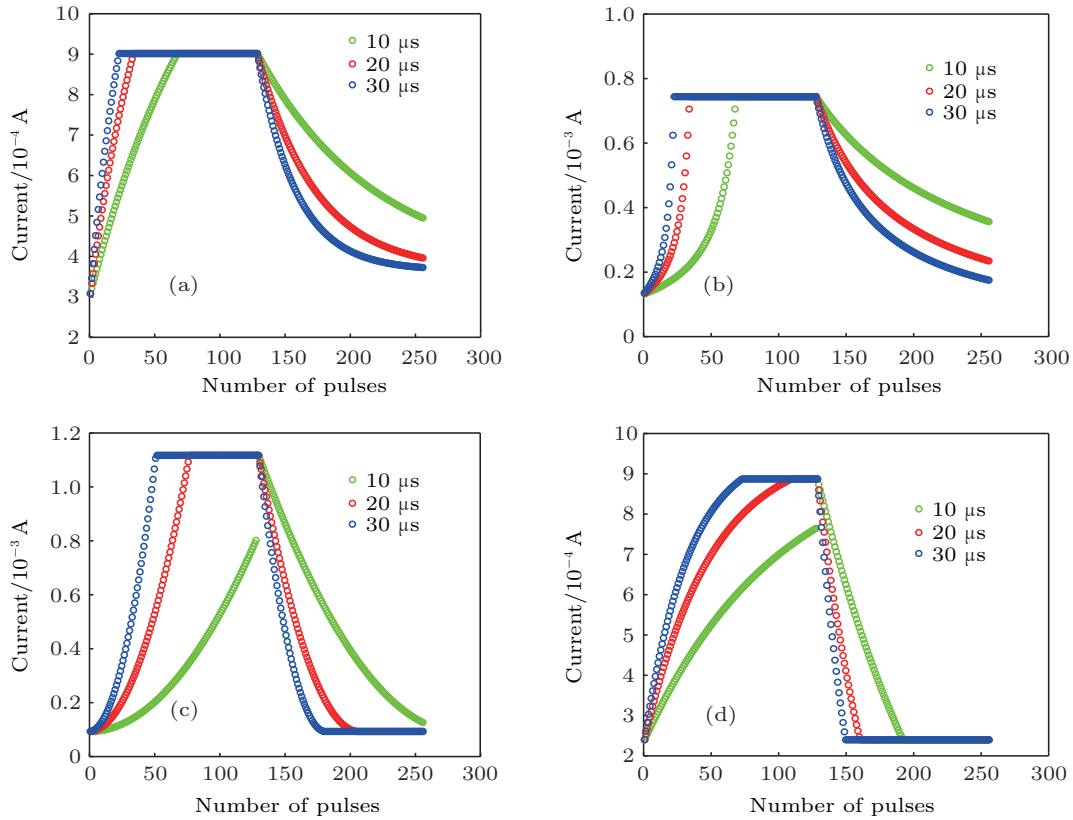


Fig. 6. (color online) Simulation of the memristive models with identical voltage pulses. The pulse widths are 10 μs, 20 μs, and 30 μs, respectively. (a) The proposed model, (b) the Simmons model, (c) Chang's model, and (d) Yang's model.

In this simulation, the proposed model most effectively predicted the LTP/LTD behaviors of the device, followed by the Simmons model, Chang's model, and then Yang's model. Though these reference models have passed Linn's criteria,[19] they are not effective enough to predict the LTP/LTD behavior.

For most memristive devices, the depression operation is a gradual, controllable process. This gradual LTD behavior can be used to process grayscale images. The conductance of the device represents the gray level of a pixel. In the following subsection, we implement grayscale image processing applications based on the proposed and the Simmons models.

4.2. Image processing applications

Image processing is a data-intensive application which requires massive calculation and high efficiency. By exploiting application-specific integrated circuits (ASICs) or field programmable gate arrays (FPGAs), the efficiency of image processing can be significantly enhanced, but still cannot satisfy the requirements of many applications, e.g., real-time video monitoring, large-scale image retrieval and multi-target tracking.[3,43] In this subsection, we explore gray sketching and edge detection based on memristive models using Matlab. In Fig. 7, a memristor-based network for image processing is shown.[44] There are three layers, including pre-processing, processing and output. The processing layer is amplified in the upper right corner of the figure. The forced pulse width is fixed to 20 μs, but the pulse amplitude is variable. Each device is initially at the LRS state. Detailed simulation results of the LTP/LTD behavior based on the memristive models are shown in Fig. 6.

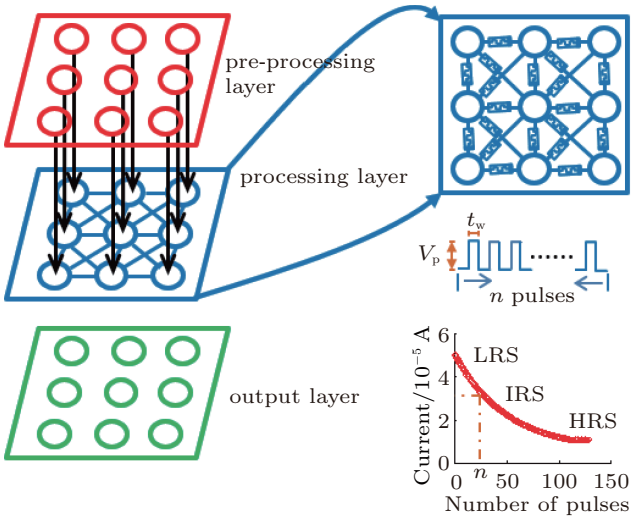


Fig. 7. (color online) Memristor-based network for image processing described. Potentiation: voltage amplitude 0.55 V, time width 25 μs, rise and fall times 100 ns. Depression: voltage amplitude −0.7 V, time width 20 μs, rise and fall times 100 ns.

4.2.1. Gray sketching

Gray sketching is a basic gray level transformation to enlarge gray level dynamic range that can be divided into linear and nonlinear transformation methods. The former transformation is always oversimplified and not effective, whereas the latter tends to be complex and time-consuming. Here, we propose a novel nonlinear transformation approach, which does not require the calculation of standard deviation or other complex nonlinear functions, and therefore can greatly enhance the efficiency of the transformation. The approach consists of four steps: first, calculate mean gray level g_{m} of a grayscale image in the pre-processing layer. Second, for each pixel, acquire the absolute difference g_{d} between its gray level and g_{m}, and also keep the sign s_{d} of the difference in the pre-processing layer. Third, apply g_{d} voltage pulses to the corresponding device at the initial LRS state in the processing layer. Finally, calculate the transformation result by the following equation in the output layer:

$$g_{\mathrm{str}} = \mathrm{round}\left(128 s_{\mathrm{d}} \frac{c_{\mathrm{LRS}} - c_{\mathrm{IRS}}}{c_{\mathrm{LRS}} - c_{\mathrm{HRS}}} + g_{\mathrm{m}}\right), \tag{10}$$

where c_{LRS}, c_{HRS}, and c_{IRS} represent the conductance of the proposed model at the LRS, HRS, and intermediate resistance states (IRS). The calculation of c_{IRS} contains the running time of a subtraction operation (2^{nd} step), calculating the absolute value (2^{nd} step), and the forced voltage pulses (3^{rd} step).

In Fig. 8, we apply the proposed and the Simmons models to image processing. Figure 8(a) is the original Lena image with the size of 256×256. Figure 8(b) is the gray sketching result of a traditional nonlinear method and figures 8(c) and 8(d) are the results of our new method based on the proposed model and the Simmons model at applied pulse amplitudes of 1.0 V and 1.3 V, respectively. We use standard deviation to measure the contrast ratio (CR) of an image.[45] The CRs of Figs. 8(a)–8(d) are 47.7, 64.0, 77.0, and 73.4, respectively. Comparing to the original image, they all have greatly enhanced the CR. In Fig. 9, the relationships between the CRs and the applied pulse amplitudes corresponding to both models are shown. The initial CR is 47.7. As the pulse amplitude increases, the CRs corresponding to the proposed model remain constant before reaching 0.72 V, and after that, the CRs begin to increase rapidly, exhibiting a threshold-like behavior, while the CRs corresponding to the Simmons model continue to demonstrate a gradual and linear growth. This threshold-like behavior is an advantage that can be utilized to restrain the unavoidable noise in applied signal.

The new method avoids time-consuming calculation of the complex nonlinear functions required by common nonlinear transformation method and it may further save time due to its physical hardware implementation.

4.2.2. Edge detection

Edge points are important features both in image processing and computer vision fields, which represent sudden gray

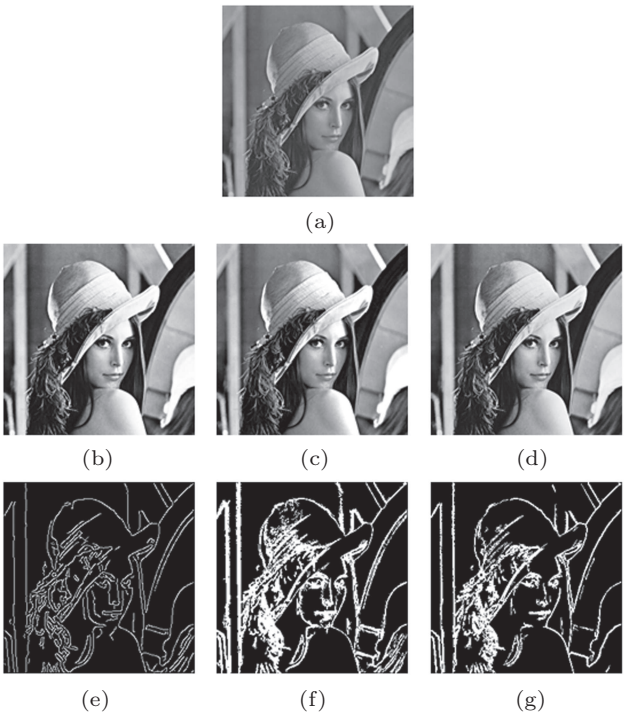


Fig. 8. Applying the memristive models to image processing. (a) Original Lena image, (b) traditional gray sketching method, (c) and (d) proposed gray sketching method based on the proposed and the Simmons models, (e) Canny edge detection method, and (f) and (g) proposed edge detection method based on the proposed and the Simmons models.

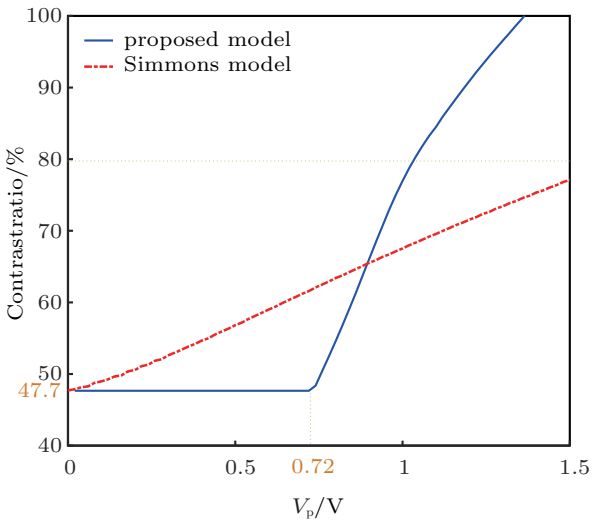


Fig. 9. (color online) Contrast ratios of processed image under applied voltage pulses with different amplitudes.

level variations. Here, we propose a novel method which utilizes the LTD behavior based on memristive models to perform edge detection operation. Similar to the method discussed in the previous subsection, the proposed method avoids the calculation of complex functions and is highly efficient.

For two adjacent pixels in a grayscale image, first, we calculate the absolute difference n_d of their gray levels in the pre-processing layer. Second, we apply n_d identical voltage pulses to the corresponding device at the initial LRS state and record the conductance of intermediate resistance state c_{IRS} in the processing layer. Third, we calculate the degree of gray level variation g_{edge} of the two pixels by the following equation in the output layer:

$$g_{edge} = \text{round}\left(256\frac{c_{LRS} - c_{IRS}}{c_{LRS} - c_{HRS}}\right), \tag{11}$$

and finally, we compare g_{edge} with a fixed threshold T_{edge}. If g_{edge} exceeds the threshold, the current pixel is regarded as an edge point; otherwise, it is a common point.

In Figs. 8(e)–8(g), we show edge detection results of the Lena image using Canny operator,[46] our new method based on the proposed and the Simmons models at an applied pulse amplitude of 1.3 V, with T_{edge} equals to 80. The Canny operator is a classic and accurate approach to detect edge points, so its detection result can be a standard. A comparison of the memristive models in edge detection is listed in Table 3. The proportion of the false points is defined as the quotient between the number of the detected edge points undetected by the Canny operator and the number of the whole points in the image. The new method based on the proposed model detects 3.79% more edge points than that of the Simmons model at a cost of detecting 1.57% more false edge points. False edge points concentrate on the neighborhood of real edge points and a simple thinning method can eliminate most of the false points.

Further comparisons of the memristive models in edge detection at different voltage thresholds are shown in Figs. 10 and 11. In Fig. 10, the letter "P" in the inset represents the proposed model and "S" represents the Simmons model. The solid lines with different colors show the point ratios corresponding to the proposed model under different pulse amplitudes, and accordingly, the dash lines correspond to the Simmons model.

The types and colors of the lines in Fig. 11 have identical representations as those in Fig. 10. The basic trend is that, as the voltage threshold increases or the applied voltage amplitude decreases, both the edge point detection ratio and the false point ratio decrease. At the applied voltage amplitudes of 1.2 V and 1.3 V, the edge point detection ratios corresponding to the proposed model are relatively higher than the ones corresponding to the Simmons model at a cost of detecting more false edge points.

Table 3. Comparison of the proposed and the Simmons models in edge detection.

Points	Canny operator	Proposed model		The Simmons model	
		Points	Proportion/%	Points	Proportion/%
Edge points	6133	5019	81.84	4787	78.05
False points	/	10833	16.53	9804	14.96

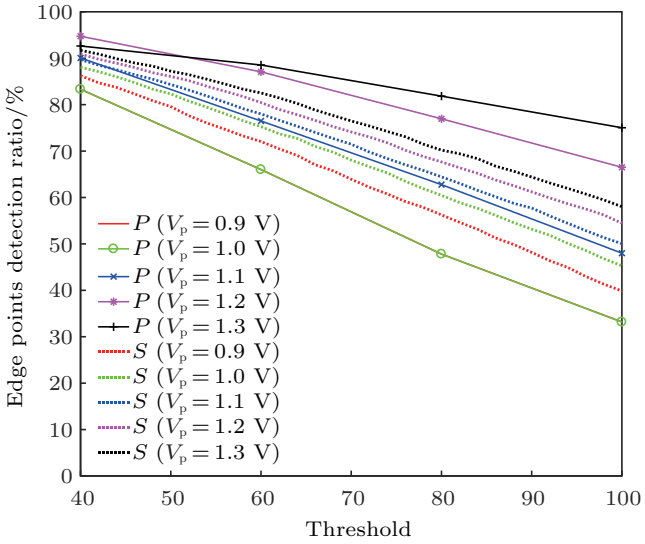


Fig. 10. (color online) Edge points detection ratios at different gray level thresholds.

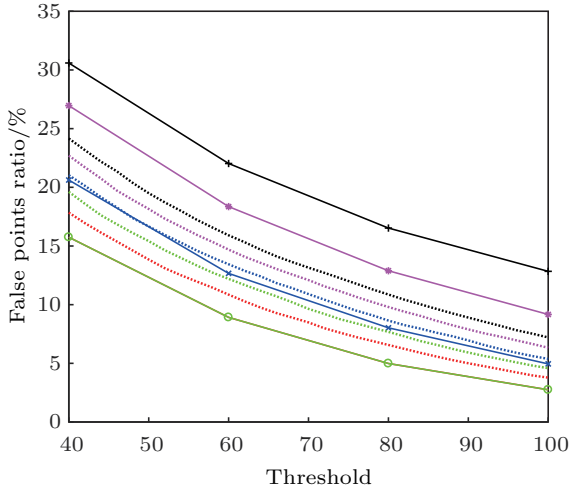


Fig. 11. (color online) False points ratio at different gray level thresholds.

Consequently, the new method based on the proposed model exhibits better detection results over the same method based on the Simmons model. Our method locates the edge points efficiently with continuity and accuracy, and therefore can be a template for how to tackle the efficiency problem of image processing using a memristor-based network.

5. Conclusion and perspectives

A novel experiment-based memristive model has been presented which considers the drifting effect, the diffusing effect, and the NDR effect. This physics-oriented model was obtained after extensive study of the physical mechanisms of fabricated TiO_x-based devices. The proposed model passes Linn's criteria, and the characteristics of flexibility, generality and accuracy have been fully verified.

The proposed model along with memristive models previously reported has been fit to experimental data by tuning the parameters to minimize RMS and TAE error functions. During this fitting, the proposed model without NDR has higher accuracy and efficiency compared to the memristive models previously reported. Further, the proposed model exhibited high generality and accuracy when fitted to the HfO_x-based device, TaO_x-based device, and the memristive models previously reported.

A prediction of LTP/LTD behavior in memristive device has been simulated based on memristive models, which could be an additional evaluation criterion of Linn's criteria. A higher predictability of the LTP/LTD behavior of the proposed model over the previous memristive models has been discovered.

Finally, based on the LTD behavior of the memristive models, two novel methods have been proposed to implement gray sketching and edge detection, which have greatly enhanced the efficiency by avoiding time-consuming calculation of complex nonlinear functions. Simulation results reveal the considerable potential for the memristor-based network to enhance the efficiency of image processing. Limited by the poor yield rate of the fabricated devices and the device-to-device variations, the physical implementation of the memristor-based network has not been completed yet and is left as a future work.

Acknowledgment

The authors thank Donald Kline, Jr for his thorough language and grammatical revisions, Shahar Kvatinsky and Misbah Ramadan for their helpful comments on the optimization procedure, and Rulin Liu and Songlin Liu for other useful comments.

References

[1] Hwang C S 2015 *Adv. Electron. Mater.* **1** 1400056
[2] Sonka M, Hlavac V and Boyle R 1993 *Image Processing, Analysis and Machine Vision* (1st edn.) (Stanford: Cengage Learning) pp. 193–242
[3] Strukov D B and Likharev K K 2007 *IEEE Trans. Nanotechnol.* **6** 696
[4] Strukov D B, Snider G S, Stewart D R and Williams R S 2008 *Nature* **453** 80
[5] Yang J J, Strukov D B and Stewart D R 2013 *Nat. Nanotechnol.* **8** 13
[6] Liu S, Sen N and Zhao X 2016 *Adv. Mater.* **28** 10623
[7] Alibart F, Zamanidoost E and Strukov D B 2013 *Nat. Commun.* **4** 2072
[8] Chai X L, Gan Z H, Lu Y, Zhang M H and Chen Y R 2016 *Chin. Phys. B* **25** 100503
[9] Chai X L, Gan Z H, Yuan K, Lu Y and Chen Y R 2017 *Chin. Phys. B* **26** 020504
[10] Chi P, Li S, Zhang T, Zhao J and Liu Y 2016 *International Symposium on Computer Architecture,* June 18–22, 2016, Seoul, Korea, p. 27
[11] Bao B C, Hu H W, Liu Z and Xu J P 2014 *Chin. Phys. B* **23** 070503
[12] Liu W, Wang F Q and Ma X K 2015 *Chin. Phys. B* **24** 118401
[13] Pickett M D, Strukov D B and Borghetti J L 2009 *J. Appl. Phys.* **106** 074508
[14] Kvatinsky S, Friedman E G and Kolodny A 2013 *IEEE Trans. Circ. Syst. I* **60** 211
[15] Chang T, Jo S H, Kim K H, Sheridan P and Gaba S 2011 *Appl. Phys. A* **102** 857

[16] Kvatinsky S, Friedman E G and Kolodny A 2015 *IEEE Trans. Circ. Syst. II* **62** 786
[17] Yang J J, Pickett M D and Li X 2008 *Nat. Nanotechol.* **3** 429
[18] Yakopcic C and Taha T M 2013 *IEEE Trans. Comput. Aided Des. Integr. Circuits Syst.* **32** 1201
[19] Linn E, Siemon A and Waser R 2014 *IEEE Trans. Circ. Syst. I* **61** 2402
[20] Yuan F, Wang G Y and Wang X Y 2015 *Chin. Phys. B* **24** 060506
[21] Wang X P, Min C and Yi S 2015 *Chin. Phys. B* **24** 088401
[22] Pickett M D, Julien B and Yang J J 2011 *Adv. Mater.* **23** 1730
[23] Szot K, Rogala M and Speier W 2011 *Nanotechnol.* **22** 254001
[24] Rainer W, Regina D and Georgi S 2009 *Adv. Mater.* **21** 2632
[25] Tang Z, Fang L and Xu N 2015 *J. Appl. Phys.* **118** 185309
[26] Linn E, Rosezin R, Kügeler C and Waser R 2010 *Nat. Mater.* **9** 403
[27] Xu N, Fang L and Chi Y 2014 *Proc. IEEE Int. Conf. Nanotechol.*, August 18–21, 2014, Toronto, Canada, p. 727
[28] Chua L O 1971 *IEEE Trans. Circuit Theory* **18** 507
[29] Chua L O and Kang S M 1976 *Proc. IEEE* **64** 209
[30] Salaoru L, Li Q, Khiat A and Prodromakis T 2014 *Nanoscale Res. Lett.* **9** 552
Li J, Tang A and Li X 2014 *Nanoscale Res. Lett.* **9** 1040
[31] Russo U, Kalamanathan D, Ielmini D, Lacaita A L and Kozicki M 2009 *IEEE Trans. Electron Devices* **56** 1040
[32] Yu S and Wong H S P 2011 *IEEE Trans. Electron Devices* **58** 1352
[33] Ielmini D 2011 *IEEE Trans. Electron Devices* **58** 4309
[34] Linn E, Menzel S, Ferch S and Waser R 2013 *Nanotechnol.* **24** 384008
[35] Van D H, Havel J V and Linn E 2013 *Sci. Rep.* **3** 2856
[36] Snyman J 2005 *Practical Mathematical Optimization* (New York: Springer Science and Business Media) p. 97
[37] Brooks S P and Morgan B J T 1995 *The Statistician* **44** 241
[38] Covi E, Brivio S and Serb A 2016 *Proc. IEEE Int. Symp. Circ. Syst.*, May 22–15, 2016, Montreal, Canada, pp. 393–396
[39] Siemon A, Menzel S and Marchewka A 2014 *Proc. IEEE Int. Symp. Circ. Syst.*, June 1–5, 2014, Melbourne, Australia, pp. 1420–1423
[40] Jang J W, Park S and Jeong Y H 2014 *Proc. IEEE Int. Symp. Circ. Syst.*, June 1–5, 2014, Melbourne, Australia, pp. 1054–1057
[41] Brivio S, Covi E and Serb A 2016 *Appl. Phys. Lett.* **109** 133504
[42] Covi E, Brivio S and Serb A 2016 *Front. Neurosci.* **10** 482
[43] Kim K, Li S and Kim J Y 2009 *IEEE Trans. Circ. Syst. Video Technol.* **19** 1612
[44] Liu Y and Wang L 2014 *Acta Phys. Sin.* **63** 080503 (in Chinese)
[45] Peli E 1990 *JOSA* **7** 2032
[46] Canny J 1986 *IEEE Trans. Pattern Anal. Mach. Intell.* **PAMI-8** 679